Macromolecular Materials and Engineering
www.mme-journal.de

Enhanced Solid Particle Erosion Properties of Thermoplastic Polyurethane-Carbon Nanotube Nanocomposites

Mengyao Dong, Chuan Wang, Hu Liu, Chuntai Liu*, Changyu Shen, Jiaoxia Zhang, Chengxinzhuo Jia*, Tao Ding*, and Zhanhu Guo**

A co-coagulation method combined with hot pressing technique is successfully applied to fabricate thermoplastic polyurethane (TPU) nanocomposites with different contents of carbon nanotubes (CNTs). Obviously, the mechanical and thermal properties of the nanocomposites are improved with increasing the CNT content. In addition, the existence of hydrogen bonding between CNTs and polymer matrix is demonstrated. Furthermore, the influences of impact parameters on solid particle erosion behavior are investigated systematically. The surface roughness and line roughness are also investigated to illustrate the mechanism of solid particle erosion. As elastic nanocomposites, the maximum and minimum erosion rate (ER) occur at 30° and 90°. The ER is relatively small when the impact velocity is at 10 m s^{-1}, then is increased rapidly between 20 and 30 m s^{-1}. As the size of impact particles increases to 300 µm, a rapid increase of ER occurs between 10 and 20 m s^{-1}. All these results indicate CNTs improve the erosion resistance of TPU matrix.

1. Introduction

Since the pioneering work done by Reynolds in 1873,[1,2] the categories and mechanisms of solid particle erosion have been continuously studied. For example, Hutchings and Bitter defined the solid particle erosion as material damages caused by the repeated impact of small particles against material surface.[3,4] Finnie and Meng reviewed the existing solid particle erosion categories in 1995, respectively.[5,6] The influencing parameters of solid particle erosion revealed the complexity of the phenomenon.[7–17] Although the study of solid particle erosion has a long history, there are still some challenges urged to be solved, including the design and manufacturing of the anti-erosion materials, and the establishment of general mathematical models of erosion under different erosion conditions.

During the last decades, polymers and their composites have been continuously displacing the conventional materials, due to their relatively simple processability, low manufacturing cost, and outstanding corrosion resistance.[18–25] The enhanced physical, chemical, and engineering properties make these materials widely used in the industrial fields, to be specific, the fabrication of the helicopter rotors, wind turbine blades, water blades, aircrafts, sensors, electromagnetic interface (EMI) shielding, and pipelines.[26–40] In a series of polymers, a segmented copolymer thermoplastic polyurethane (TPU) with hard and soft blocks attracts tremendous attention for both scientific research and industrial applications.[41] TPU is regarded as a self-reinforcing

M. Dong
School of Materials Science and Engineering
Zhengzhou University
Zhengzhou, 450002 Henan, China
M. Dong, C. Wang, Dr. H. Liu, Prof. C. Liu, Prof. C. Shen
National Engineering Research Center for Advanced Polymer Processing Technology
Zhengzhou University
Zhengzhou 450002, China
E-mail: liuhu@zzu.edu.cn; ctliu@zzu.edu.cn
Prof. J. Zhang
School of Material Science and Engineering
Jiangsu University of Science and Technology
Zhenjiang 212000, China
The ORCID identification number(s) for the author(s) of this article can be found under https://doi.org/10.1002/mame.201900010.
Prof. C. Jia
Eco-development Academy
Southwest Forestry University
Kunming Yunnan 650224, China
E-mail: jiachenxinzhuo@126.com
Prof. T. Ding
College of Chemistry and Chemical Engineering
Henan University
Kaifeng 475004, China
E-mail: dingtao@henu.edu.cn
M. Dong, Prof. Z. Guo
Integrated Composites Laboratory (ICL)
Department of Chemical & Biomolecular Engineering
University of Tennessee
Knoxville, TN, 37996 USA
E-mail: zguo10@utk.edu

DOI: 10.1002/mame.201900010

 © 2019 WILEY-VCH Verlag GmbH & Co. KGaA, Weinheim

elastomeric polymer and can be processed as plastic.[42,43] At the same time, TPU also shows an excellent erosion resistance and impact absorbing properties.[44–46] These advantages make TPU suitable for the production of anti-erosion films or coatings.

To improve the performance, a common method is the addition of appropriate nanofillers into polymer matrix.[47–65] Compared with neat TPU, the addition of carbon-based nanoparticles can improve the mechanical properties and thermal stability of the composites, thereby enhancing the solid particle erosion resistance of the composite. Furthermore, one of the important features that determines the improvement in the performance of nanocomposites is the dispersivity of nanoparticles in the polymer matrix. Generally, matrix-filler compatibility, surface energy of the particles, and processing techniques are the key factors to influence the dispersion of fillers. Although solution mixing techniques have the disadvantages of slow polymerization rate, solvent consumption, solvent recovery, and low equipment utilization, its good dispersibility still makes it widely used. Coagulation technique (one of the solution mixing techniques) is a technique to precipitate the polymer from its solution by adding the poor solvent for polymer dissolution. Thus, "co-coagulation" was used to describe this process. In this work, CNTs/TPU mixture was added into the poor solvent methanol of TPU and CNTs/TPU nanocomposites precipitated together, keeping the good dispersion of CNTs in the TPU matrix. The effects of carbon black (CB) on the TPU erosion performance was previously studied.[2] However, compared with CB, CNTs have a larger specific surface area and can be combined with polymer matrix more effectively. Adding a lower content of CNTs to a polymer matrix can match the performance of a composite with higher CB contents. Hence, the erosion mechanism of CNTs/TPU nanocomposites still needs be systematically investigated. In this study, apart from enlarging the database on the erosion behavior of CNTs/TPU nanocomposites, the other objective is to study the effects of CNTs reinforcement under different impact conditions. In this work, a co-coagulation method combined with hot pressing technique was successfully applied to fabricate the CNTs/TPU nanocomposites. In addition, the dispersion of CNTs was investigated by field emission scanning electron microscopy (FE-SEM), and transmission electron microscopy (TEM). In order to confirm the existence of the interactions between CNTs and TPU matrix, the results of Fourier transform infrared spectroscopy (FTIR) and Differential scanning calorimetry (DSC) were recorded. The mechanical and thermal properties were characterized respectively, and their relationships with solid particle erosion resistance were revealed.

2. Experimental Section

2.1. Materials and Chemicals

The CNTs (TNIM8) with a density of 2.1 g cm^{-3} were purchased from Chengdu Organic Chemicals Co., Ltd. TPU (Elastollan 1185A) with a density of 1.12 g cm^{-3} was obtained from BASF Co., Ltd. The CNTs and TPU were dried at 80 °C for 24 h in a vacuum oven before use. Dimethylformamide (DMF) and methanol were purchased from Zhiyuan Reagent Co., Ltd, China.

2.2. Preparation

A co-coagulation method combined with hot pressing technique was successfully applied to fabricate the CNTs/TPU nanocomposites (**Figure 1**). First, magnetic stirring for 30 min at 40 °C was used to dissolve 3.0 g TPU in 50 mL DMF. To disperse CNTs homogenously, a suitable amount of CNTs was ultrasonicated in 15 mL DMF for 30 min. In the second step, the two solutions were mixed and ultrasonicated for another 30 min. In order to obtain the flocculate of CNTs/TPU, the mixed solution was dropped into 300 mL methanol. The flocculated CNTs/TPU were filtered and then dried in a vacuum oven for 24 h at 80 °C. The samples of 0.4 mm thick CNTs/TPU nanocomposite films were produced by hot pressing at 200 °C for 8 min under a pressure of 10 MPa. In order to distinguish, the CNTs/TPU nanocomposites were denoted as TPU-*x*CNTs, where *x* represented the mass fraction of CNTs.

2.3. Characterization

The FTIR spectra from 500 to 4000 cm^{-1} were carried out using a Nicolet Nexus 870 instrument. A TA instruments Q 2000 was used to conduct the DSC analysis under N_2 atmosphere and each sample was scanned at a heating rate of 10 °C min^{-1} in the range of 40 to 220 °C. The mechanical properties were investigated on an electrical universal testing machine (UTM2203). The samples (40 mm × 4 mm × 0.4 mm) were tested at the strain rate of 0.1 min^{-1}. The morphologies of CNTs in TPU and erosion surfaces were observed using SEM (FEI Nova NanoSEM 450) and TEM (JEM-1230) instrument. The surface roughness of all grids (1000 μm × 1000 μm) was measured using a Leica digital microscope (DVM6), the data were plotted in a figure to illustrate the surface roughness. A Hot Disk instrument (TPS2200, Sweden) was used to measure the thermal

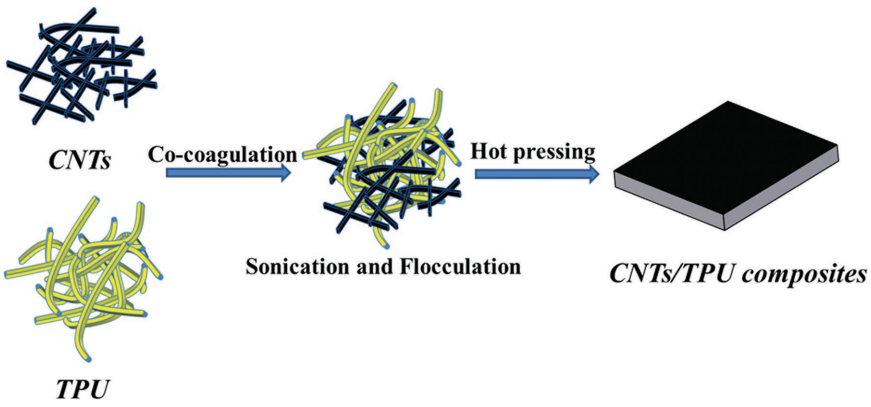

Figure 1. Schemes for the fabrication of CNTs/TPU nanocomposites by co-coagulation technique and hot pressing.

© 2019 WILEY-VCH Verlag GmbH & Co. KGaA, Weinheim

conductivity of the test samples (20 mm × 4 mm × 0.4 mm). A Thermogravimetric analysis (TGA) instruments (Q50) was used to carry out the thermal stability of the test samples under N_2 atmosphere from room temperature to 700 °C with a heating rate of 10 °C min^{-1}. A sand-blasting instrument (BH-1350, Shenzhen Datong Co., Ltd) was used to study the erosion performance for the sample (20 mm × 4 mm × 0.4 mm) which was tightly attached to a stainless steel plate. In order to describe solid particle erosion performance better, erosion rate (ER) was defined from the weight loss of the sample due to the weight of the erodent as the following formula[2]:

$$\mathrm{ER} = \frac{W_m}{W_p} \tag{1}$$

where W_m is the weight loss of CNTs/TPU film and W_p is the weight of the impact particles (testing time × feed rate), and the weight of CNTs/TPU film was recorded by precision balance.

3. Results and Discussion

3.1. Microstructure

In general, CNTs tend to be entangled in polymer matrix.[66,67] This entanglement phenomenon seriously affects the integrity of composites. **Figure 2** depicts the freeze-fractured surface of CNTs/TPU nanocomposites. As shown in Figure 2a–c, the individual CNTs were uniformly dispersed in the polymer matrix. Meanwhile, TEM micrographs were used to further identify the good dispersion of CNTs, in Figure 2d–f, the direct evidence for uniformly dispersed CNTs was observed. Neither CNT showed a significant agglomeration in either the SEM photographs or the TEM images. Hence, the ultrasonic treatment during the fabrication procedure was beneficial for the dispersion.

3.2. Interfacial Interaction

It is well known that the groups on CNTs (O–H peak at 1630 and 3400 cm^{-1} in **Figure 3**a) can form hydrogen bonds with functional groups on the TPU chains. Although the van der Waals interaction between CNTs could cause the entanglement, the hydrogen bonds between CNTs and TPU chains could strengthen the mechanical properties of nanocomposites.[68,69] In this work, we introduced the hydrogen bonding index (R: ratio of two peaks at 1700 and 1730 cm^{-1}) to illustrate the change of hydrogen bonds between CNTs and TPU chains.[70] As shown in Figure 3a and **Table 1**, the hydrogen bonding index R increases from 0.654 for TPU to 0.848 for TPU-3CNTs. With the increase of hydrogen bonds, the combination of CNTs and TPU matrix will gradually increase, and enhance the mechanical performance of CNTs/TPU. Besides FTIR, the glass transition temperature (T_g) also accounts for the interaction between the reinforcement and the matrix.[71] As shown in Figure 3b, the T_g decreases from –27.35 to –29.36 °C. The free volume between the soft segments of the TPU is known to determine the T_g. On one hand, the addition of CNTs changes the molecular chain configuration in the TPU matrix, and the originally tightly packed molecular chain packing pattern is disturbed, and a large amount of space for the molecular chain to move freely is formed around the CNTs, that is, the free volume increases. On the other hand, an increase in the free volume causes an increase in the mobility of a part of the molecular chain to lower the T_g.[72–76] In other words, the CNTs increased the distance between the soft segments of the TPU chains, resulting in an increase in free volume and easy movement of the segments, so the T_g tends to decrease. In addition, the addition of CNTs hinders the crystallization of the TPU hard segment molecular chain, resulting in a reduction in the size of the molecular chain. The binding of the hard segment as a physical cross-linking point to the soft segment molecular chain will be weakened, thereby increasing the mobility of the soft segment molecular chain, so the T_g of the nanocomposites will decrease. The same result was found in other composite systems.[42,71,77,78]

3.3. Mechanical Properties

The stress–strain curves of CNTs/TPU nanocomposites are shown in **Figure 4**. Compared to the neat TPU (4.688 MPa), the

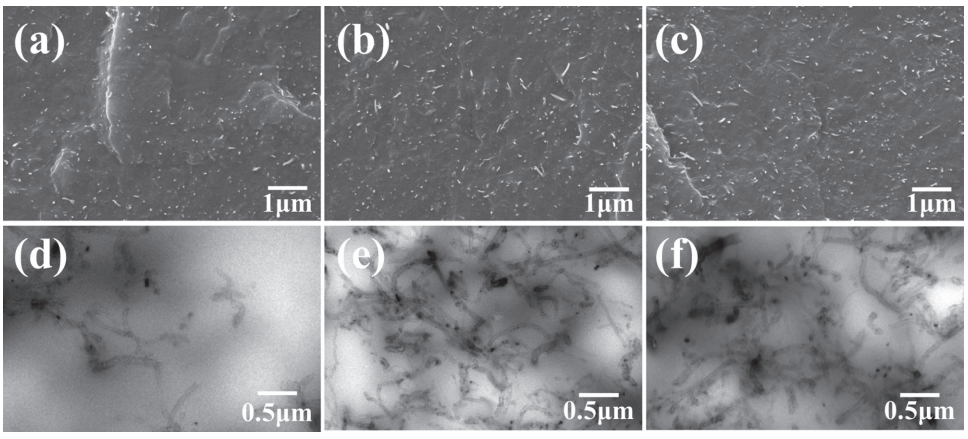

Figure 2. Fe-SEM image of the freeze-fractured surface of a) TPU-1CNTs, b) TPU-2CNTs, c) TPU-3CNTs; and TEM micrograph of d) TPU-1CNTs, e) TPU-2CNTs, f) TPU-3CNTs.

© 2019 WILEY-VCH Verlag GmbH & Co. KGaA, Weinheim

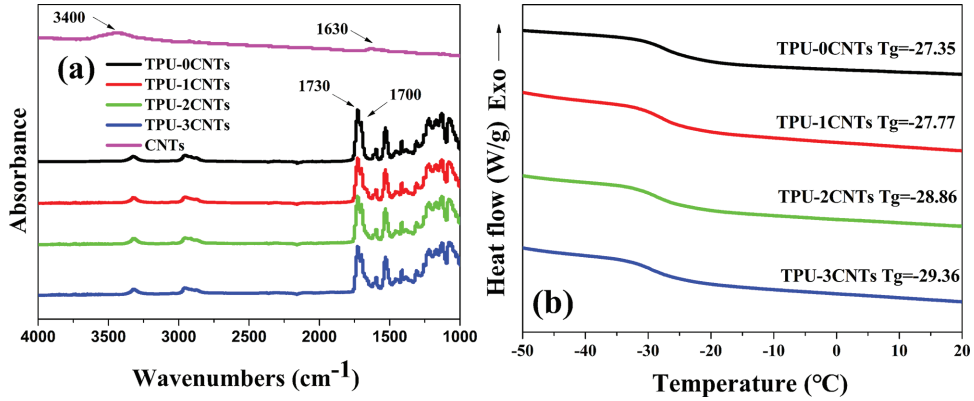

Figure 3. a) FTIR spectra, b) DSC curves of CNTs/TPU nanocomposites.

Table 1. Hydrogen bonding indexes (R) of CNTs/TPU nanocomposites.

Sample	Hydrogen bonding indexes [R]
TPU-0CNTs	0.654
TPU-1CNTs	0.780
TPU-2CNTs	0.819
TPU-3CNTs	0.848

tensile strength is observed to be 5.466, 6.872, and 7.575 MPa for CNTs/TPU nanocomposites, respectively. Compared with the CB/TPU nanocomposites, the tensile properties are greatly improved when the content of CNTs is small. The TPU-1CNTs have an improvement in tensile properties equivalent to TPU-6CB (5.404 MPa). Compared to TPU-6CB, the tensile property of TPU-3CNTs was increased by 40.17%.[2] The Young's modulus increased with the increase of CNTs content in the TPU, and the change in elongation at break showed the same tendency as the Young's modulus. The elongation at break of the TPU-1CNTs (65.5%) was basically the same as the TPU-6CB (65.49%). Compared to TPU-6CB, the elongation at break of TPU-3CNTs was increased by 13.84%.[2] There are many factors affecting the mechanical properties of polymer matrix composites, including the dispersion of fillers, the combination of fillers and polymer matrix, crack propagation, force transfer, energy dissipation, and so on.[79–81] As expected, the key factor for improving the mechanical performance is the dispersion of the reinforcement in the polymer matrix.[82] Figures 2 and 3 provide strong evidences to support this conclusion. During the deformation process, stress concentration occurs around the evenly dispersed CNTs, causing the polymer matrix around the reinforcement to yield and absorb a large amount of deformation energy. Simultaneously, the evenly dispersed CNTs and TPU chains were linked together to form a network structure through the interface layer, the cross-linking points could transfer stress and prevent the expanding of cracks.[83] Moreover, the functional groups of the CNTs could form chemical bonds with the polymer chains. When the CNTs/TPU nanocomposites were stretched, the chemical bonds were broken and absorbed the deformation energy, and thus improved the mechanical performance.

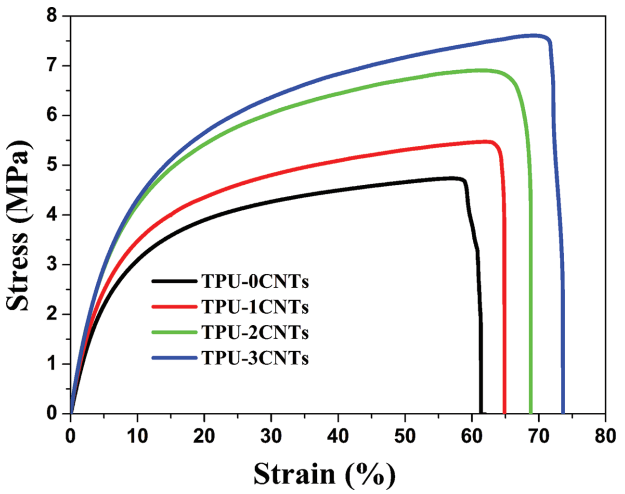

Figure 4. Representative stress-strain curves of CNTs/TPU nanocomposites.

3.4. Thermal Stability and Thermal Conductivity

Figure 5 shows the TGA and differential thermogravimetric (DTG) curves of CNTs/TPU nanocomposites. The initial decomposition temperature ($T_{5\%}$ and $T_{10\%}$) and the largest thermal decomposition temperature (T_{max}) are shown in **Table 2**. Obviously, the $T_{5\%}$, $T_{10\%}$, and T_{max} of TPU were improved by the addition of CNTs, and an improvement of 9.84, 9.00, and 13.46 °C was observed for the 3% content CNTs, respectively. First, the addition of CNTs can slow down the decomposition of the TPU matrix and prevent the diffusion of pyrolysis products and release to the outside, thereby improving the thermal stability of the composite. Second, the CNTs still contain functional groups, which can form chemical bond with TPU molecular chains.[84,85] When the nanocomposite is decomposed, it absorbs a large amount of energy to destroy the chemical bond between CNTs and the TPU chains. Hence, the CNTs enhanced the thermal stability of TPU. The thermal conductivities are shown in Table 2 as well. The thermal conductivity of TPU-1CNTs, TPU-2CNTs, and TPU-3CNTs can be increased by 21.69%, 46.00%, and 72.58% compared with that of the pure TPU, respectively. This is because of the fact that the CNTs

© 2019 WILEY-VCH Verlag GmbH & Co. KGaA, Weinheim

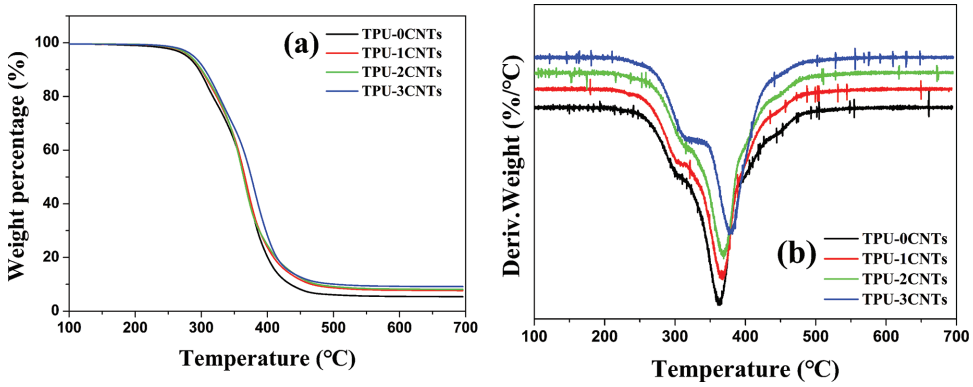

Figure 5. a) TGA and b) DTG curves of CNTs/TPU nanocomposites.

have a high thermal conductivity, and the heat conduction network is continuously improved as the content of the CNTs reinforcement increases in the matrix. Although there is a large Kapitza thermal resistance between reinforcing CNTs and TPU matrix, the thermal conductivity of the nanocomposite still shows an increasing trend. In the process of high-speed particles continuously impacting the surface of the nanocomposites, a large amount of heat is generated by collision, extrusion, and friction, so that the temperature of the nanocomposites may be greatly increased in a short time, causing the destruction or even melting of the material. Therefore, improving the thermal conductivity of the CNTs/TPU nanocomposites is beneficial to reduce the damage of the material during the erosion process. In other words, a suitable thermal conductivity can enhance the solid particle erosion performance of the material as well.

3.5. Solid Particle Erosion Behavior

The solid particle erosion performances of CNTs/TPU under different impact conditions were investigated. The results are shown in **Figure 6**. Obviously, the impact velocity has a strong influence on the ER. The ER is relatively small and maintains a certain range when the impact velocity is at 10 m s^{-1}. The sudden increase of ER occurs at 20–30 m s^{-1} when the erodent size is 100 and 150 µm. As the size of the erosion particles increases (300 µm), the sudden increase of ER occurs at 10–20 m s^{-1}. This is because the erosion particles with a small velocity can only cause the elastic deformation of the material. After the solid particle erosion process, the elastic deformation region returns to the state before the erosion, thus the ER is relatively small. As the velocity and the size of erosion particles increase, the initial kinetic energy gradually increases, reaching a critical state for the failure of the nanocomposites, so the ER shows a sudden increase.

Table 2. Thermal conductivity and thermogravimetric analysis data of CNTs/TPU nanocomposites.

Sample	Thermal conductivity [W mK^{-1}]	$T_{5\%}$/°C	$T_{10\%}$/°C	T_{max}/°C
TPU-0CNTs	0.2739	278.58	296.32	366.92
TPU-1CNTs	0.3333	282.85	299.67	368.72
TPU-2CNTs	0.3999	283.51	300.58	370.09
TPU-3CNTs	0.4727	288.42	305.32	380.38

In general, the maximum erosion rate of ductile and brittle materials is at 30° and 90°, respectively.[86] As an elastomer material, CNTs/TPU nanocomposites show a maximum ER at an oblique impact angle (30°) and minimum ER at 90° similar to the ductile response. This is because that during the erosion process, the initial kinetic energy of the impact particles is converted to different energy terms and the kinetic energy loss of the erosion particles also changes as the erosion angle changes. As shown in **Figure 7**, when the solid particle erosion impact angle is perpendicular to the surface of target materials, the heat dissipation consumes 30–40% and the storage energy of plastic deformation consumes 0–20% of the initial kinetic energy. Other 50–60% initial kinetic energy of the erosion particles is converted into elastic energy and into kinetic energy of the particles again during the rebound phase. Because of the friction, the erosion particles rotate and shift in the contact area when the erosion particles have a certain angle with the CNTs/TPU nanocomposite surface. The rotational energy and translational energy will account for 5–20% of the initial kinetic energy, respectively.[87,88] The deformation of the material upon particle erosion is similar to that of the perpendicular impact but additional micro-cutting and micro-plowing are observed, so the plastic deformation is expected to consume 20–70% of the kinetic energy.[87,88] Heat dissipation and storage energy of plastic deformation consume 20–30%, 0–10% of the initial kinetic energy, respectively.[87,88] The phenomena of cutting and plowing are related to the mechanical properties of a material. A better mechanical performance of a material represents a lower ER. Thus, the ER exhibited a different trend from the mechanical performance under all solid particle erosion conditions. Compared with our previous work,[2] it is not difficult to find that under the same erosion conditions, the ER of these two kinds of nanocomposites tends to be consistent with the increase of the impact angle. For example, with the impact velocity of 50 m s^{-1} and impact size of 150 µm, the ER of TPU-3CNTs is 1.6345, 1.4922, and 0.7128 mg kg^{-1} and the ER of TPU-6CB is 1.8523, 1.4630, and 0.7032 mg kg^{-1} for 30°, 60°, and 90°, respectively. The maximum difference in ER occurs when the impact angle is 30°. This shows that the CNTs/TPU nanocomposites perform better than the CB/TPU

© 2019 WILEY-VCH Verlag GmbH & Co. KGaA, Weinheim

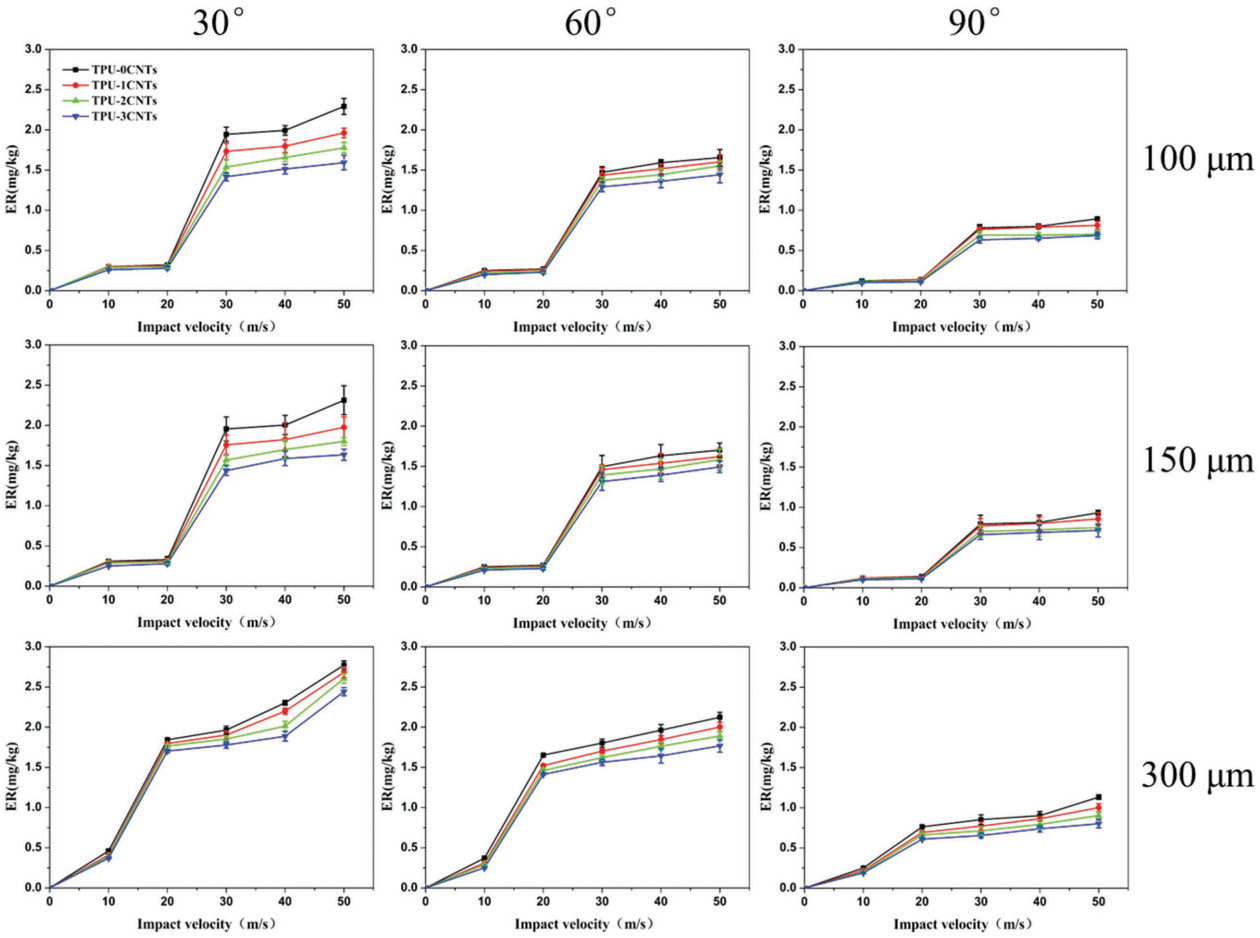

Figure 6. Erosion rate (ER) of CNTs/TPU nanocomposites as a function of impact velocity at 30°, 60°, and 90° impact angles with erodent sizes of 100, 150, and 300 μm.

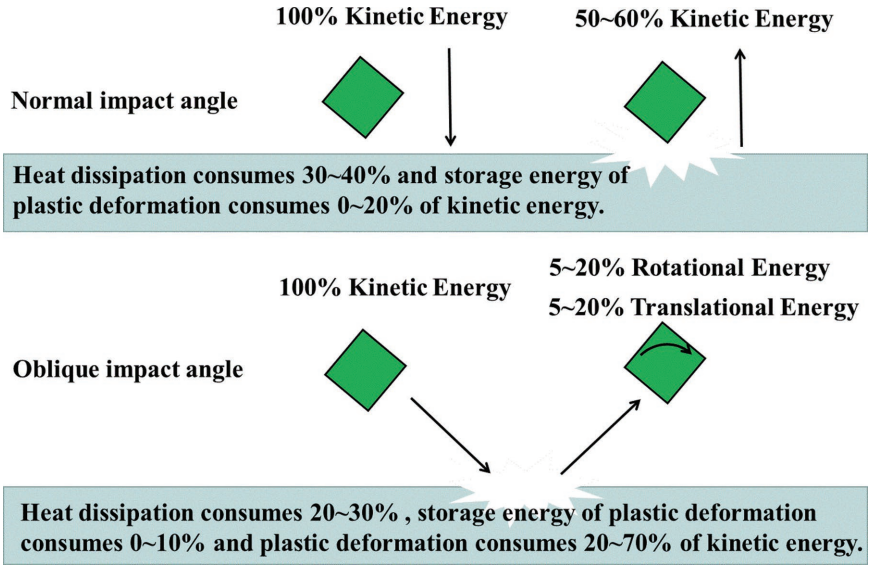

Figure 7. The kinetic energy transfer of erosion particles during solid particle erosion process.

nanocomposites at a low impact angle. At high impact angles, a better performance can be achieved by adding less CNTs than CB to the TPU matrix.

From a mechanical point of view, the impact force can be decomposed into two parts, that is, one parallel to the surface (F_p) and the other one vertical to the surface (F_v).[89] The F_p influences the cutting and plowing, and F_v controls the impact. Under normal circumstances, F_p plays a major role in the erosion process of the elastomer.[90] Furthermore, solid particle erosion failure mode for elastomer materials is complicated, involving surface micro-cracking, fracture, chipping off, and surface matrix removing.[91] A series of ridges were usually formed at the initial stage of solid particle erosion, which was transverse to the impact direction. The impacting solid particles slide over the surface and deform the ridges during the successive impact process, causing the growth of micro-cracks from the base of

© 2019 WILEY-VCH Verlag GmbH & Co. KGaA, Weinheim

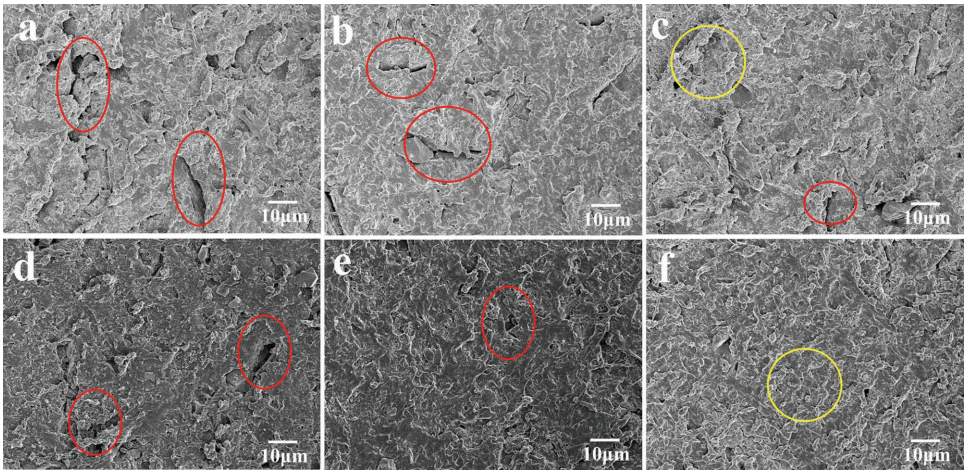

Figure 8. FE-SEM images of neat TPU (a, b, c) and TPU-3CNTs (d, e, f) after solid particle erosion of impact velocity at 30 m s^{-1} with erodent size of 150 μm, impact time of 300 s and impact angles of (a, d) 30°; (b, e) 60 ° and (c, f) 90°.

each ridge. Then the micro-cracks will grow progressively into the surface due to the frictional forces from the impact solid particles.[92] As the solid particle erosion process progresses, fracture and chipping off the surface occur when these micro-cracks intersect. With the succession of solid particle impacts, the strain was gradually increased until the material was removed. In this way, the cyclic solid particle impact caused the cracks expansion and material loss.

The surfaces of CNTs/TPU nanocomposites after solid particle erosion were observed by SEM. As shown in **Figure 8**, some plowing and cracks are marked by red circles, and plastic deformations are marked by yellow circles. The plowing, cracks, and plastic deformation caused by the impact particles are similar for the impingement angles of 30° and 60°, but it is more obvious at 30°. However, there is almost no plowing and cracks due to the zero F_p at 90° impingement angle. Hence, the maximum ER was achieved at 30° for CNTs/TPU nanocomposites. Compared with CNTs/TPU nanocomposites, neat TPU suffered severe erosion at all solid particle erosion conditions. It is consistent with the lowest erosion resistance as shown in Figure 6.

Furthermore, the surface roughness and the corresponding line roughness were evaluated to identify the solid particle erosion mechanisms of the nanocomposites. The data are plotted in **Figures 9** and **10** to illustrate the erosion morphologies and line roughness of TPU-3CNTs nanocomposite after different test conditions. In Figure 9, the *X*, *Y*, and *Z*-axis represent the length, width, and height information of the sample, respectively. The definitions of various surface roughness parameters are given in formulae 2–4:[93]

$$S_a = \iint_a \left| Z(x,y) \right| dx\, dy \tag{2}$$

$$S_q = \sqrt{\iint_a (Z(x,y))^2\, dx\, dy} \tag{3}$$

$$S_{sk} = \frac{1}{S_q^3} \iint_a (Z(x,y))^3\, dx\, dy \tag{4}$$

where S_a is the average surface roughness, S_q is the standard deviation roughness, S_{sk} is the surface skewness, a indicates the measured area, and $Z(x, y)$ corresponds to the height function over the measured area. The surface roughness parameters of 3CNTs-TPU after different test conditions are shown in **Table 3**. At the same impact angle and velocity, the S_a and S_q increase as the size of impact particles increases. With the increase of impact particle size, the initial kinetic energy appears increasing, the damage caused by the impact particles is also relatively large, and the peaks and valleys formed on the surface of the samples are unevenly distributed. The same increasing trend of S_a and S_q occurs when the impact velocity increases for the same reason. When the impact velocity and impact particle size are constant, the S_a and S_q gradually decrease as the impact angle increases. This is because as the impact angle increases, the F_p is gradually decreased, the cutting and plowing action is weakened, and the surface of the nanocomposite is relatively flat. Simultaneously, the $S_{sk} > 0$ indicates that the density of the peak is greater than the valley. When the impact particles have a certain angle with the nanocomposites surface, the cutting and plowing action of the particles causes the material accumulation, resulting in more surface peaks. In contrast, $S_{sk} < 0$ indicates that the density of the valley is greater than the peak. The S_{sk} is −1.132 when the impact angle is 90°. This shows that when the impact particles are perpendicular to the surface of the nanocomposites, the depth of the largest valley is greater than the height of the highest peak. The partial line roughness of the nanocomposite after different test conditions is shown in Figure 10, the change of line roughness shows the same trend as the surface roughness. This is consistent with the results of ER, which further illustrates the solid particle erosion mechanism of the CNTs/TPU nanocomposites.

4. Conclusion

A co-coagulation method combined with hot pressing technique was successfully applied to fabricate the CNTs/TPU nanocomposites. Obviously, the mechanical and thermal

© 2019 WILEY-VCH Verlag GmbH & Co. KGaA, Weinheim

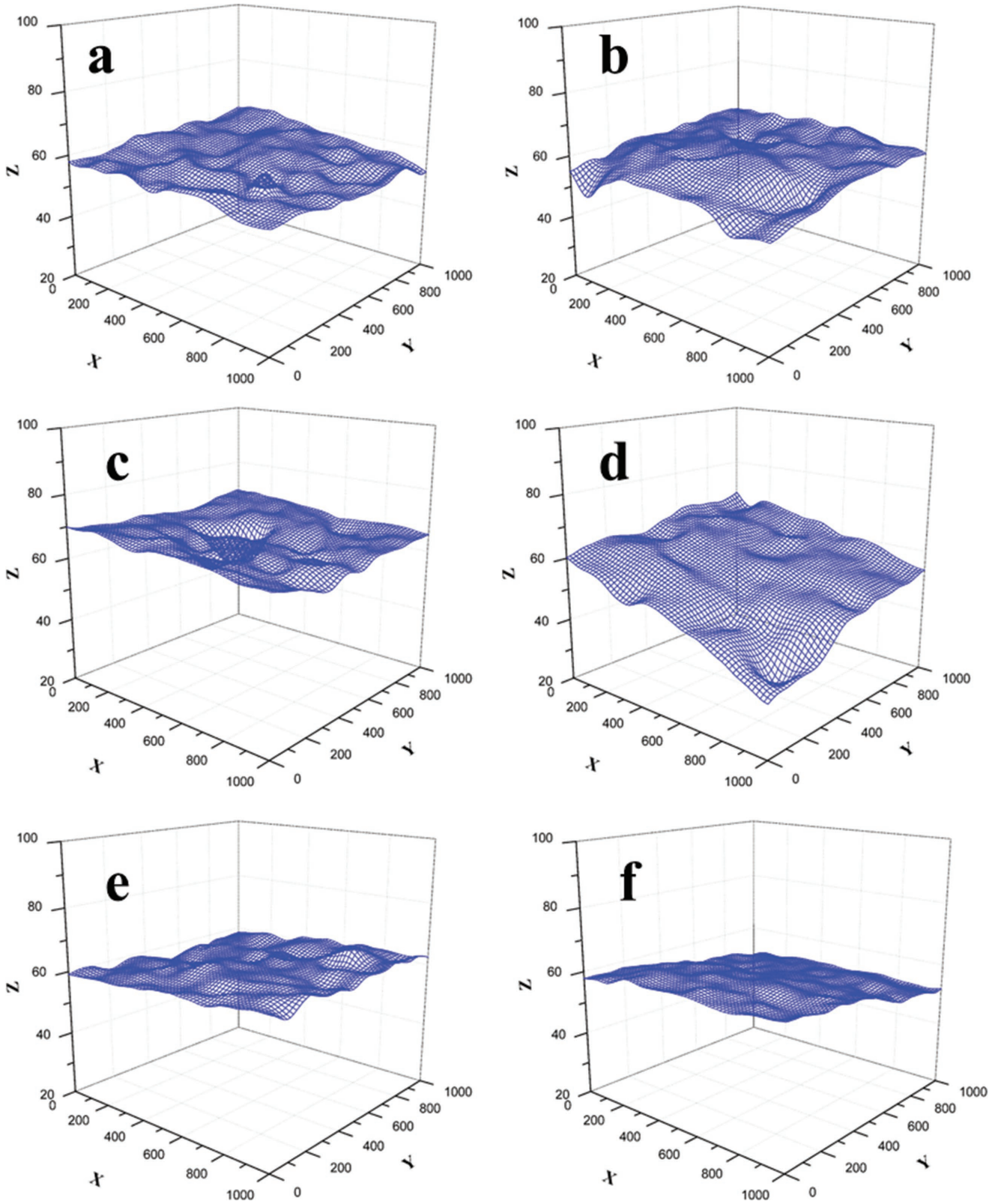

Figure 9. Erosion morphologies of TPU-3CNTs nanocomposite after different test conditions: a) impact angle 30°, impact velocity 30 m s^{-1}, impact particle size 100 μm, b) impact angle 30°, impact velocity 30 m s^{-1}, impact particle size 150 μm, c) impact angle 30°, impact velocity 30 m s^{-1}, impact particle size 300 μm, d) impact angle 30°, impact velocity 50 m s^{-1}, impact particle size 150 μm, e) impact angle 60°, impact velocity 30 m s^{-1}, impact particle size 150 μm, and f) impact angle 90°, impact velocity 30 m s^{-1}, impact particle size 150 μm.

© 2019 WILEY-VCH Verlag GmbH & Co. KGaA, Weinheim

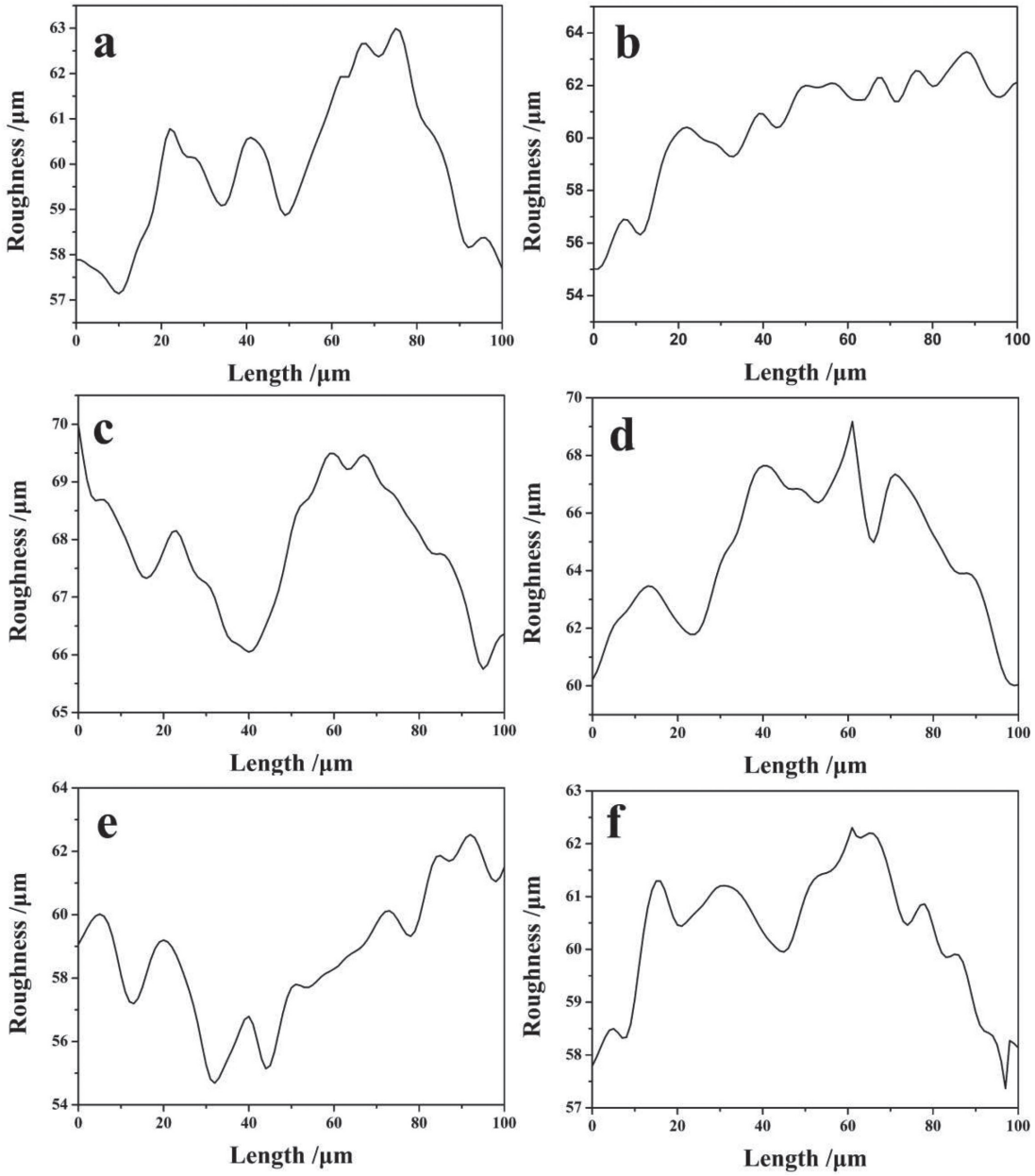

Figure 10. Line roughness of TPU-3CNTs nanocomposite after different test conditions: a) impact angle 30°, impact velocity 30 m s^{-1}, impact particle size 100 μm, b) impact angle 30°, impact velocity 30 m s^{-1}, impact particle size 150 μm, c) impact angle 30°, impact velocity 30 m s^{-1}, impact particle size 300 μm, d) impact angle 30°, impact velocity 50 m s^{-1}, impact particle size 150 μm, e) impact angle 60°, impact velocity 30 m s^{-1}, impact particle size 150 μm, and f) impact angle 90°, impact velocity 30 m s^{-1}, impact particle size 150 μm.

properties of the nanocomposites were improved with increasing the content of CNTs. In addition, the existence of hydrogen bonding between CNTs and polymer matrix was demonstrated. The hydrogen bonding index R increased from 0.654 to 0.848. Furthermore, the influences of impact parameters on the solid particle erosion behavior were investigated systematically. As elastic nanocomposites, the maximum and minimum ER occurred at 30° and 90°. The ER was relatively small when the impact velocity was at 10 m s^{-1}, then increased rapidly between 20–30 m s^{-1}. As the size of impact particles increased to 300 μm, a rapid increase of ER occurred between 10 and 20 m s^{-1}. Compared with our previous work,[2] these TPU nanocomposites with CNTs performed better than the CB/TPU nanocomposites at a low impact angle and a better erosion resistance was achieved at high impact angles by adding lower loadings of CNTs than CB to the TPU matrix. The surface roughness and line roughness also supported this conclusion. All these results indicated that CNTs improved the erosion resistance of the TPU matrix. The research will be useful in making CNTs/TPU nanocomposites applicable in the

© 2019 WILEY-VCH Verlag GmbH & Co. KGaA, Weinheim

Table 3. Surface roughness parameters of TPU-3CNTs nanocomposite.

Solid particle erosion impact parameters			Surface roughness parameters		
Angle [°]	Velocity [m s^{-1}]	Particle size [μm]	S_a/μm	S_q/μm	S_{sk}
30	30	100	1.873	2.398	0.558
30	30	150	1.986	2.457	0.641
30	30	300	2.343	2.864	0.725
30	50	150	2.521	2.933	0.744
60	50	150	1.866	2.333	0.655
90	50	150	0.684	0.884	−1.132

fields where high solid particle erosion resistances are required together with other functions such as strain sensors, EMI shielding, coating materials, etc.

Acknowledgements

The project was financially supported by National Natural Science Foundation of China-Henan Province Joint Funds (U1604253) and National Natural Science Foundation of China (11572290, 51803191). The corresponding e-mail addresses were added for H.L., C.L., C.J., and T.D. after initial online publication on February 27, 2019. The editorial office apologizes for any confusion caused.

Conflict of Interest

The authors declare no conflict of interest.

Keywords

carbon nanotubes, nanocomposite, solid particle erosion, surface roughness, thermoplastic polyurethane

Received: January 6, 2019
Revised: February 17, 2019
Published online: February 27, 2019

[1] O. Reynolds, *Philos. Mag.* **1873**, *46*, 337.
[2] M. Dong, Q. Li, H. Liu, C. Liu, E. Wujcik, Q. Shao, T. Ding, X. Mai, C. Shen, Z. Guo, *Polymer* **2018**, *158*, 381.
[3] I. M. Hutchings, R. E. Winter, *Wear* **1974**, *27*, 121.
[4] J. Bitter, *Wear* **1963**, *6*, 5.
[5] I. Finnie, *Wear* **1995**, *186–187*, 1.
[6] H. C. Meng, K. C. Ludema, *Wear* **1995**, *181–183*, 443.
[7] G. Lv, N. Zhang, M. Huang, C Shen, J. Castro, K. Tan, X. Liu, C. Liu, *Polym. Test.* **2018**, *69*, 470.
[8] R. Rattan, J. Bijwe, *Wear* **2007**, *262*, 568.
[9] S. Arjula, A. P. Harsha, *Polym. Test.* **2006**, *25*, 188.
[10] M. AminulIslam, Z. N. Farhat, *Wear* **2014**, *311*, 180.
[11] D. Mitramajumdar, H. Aglan, *Polymer* **1992**, *33*, 1855.
[12] P. H. Shipway, I. M. Hutchings, *Wear* **1994**, *174*, 169.
[13] L. W. Mckeen, *The Effect of Temperature and Other Factors on Plastics and Elastomers*, William Andrew Inc., NY **2008**.
[14] A. Kishore, G.B. Sridhar, *Polym. Test.* **2002**, *21*, 473.
[15] G. K. Drensky, *Degree Thesis*, University of Cincinnati. Cincinnati, Ohio **2002**.
[16] A. Patnaik, A. Satapathy, S. S. Mahapatra, R. R. Dash, *J. Polym. Res.* **2008**, *15*, 147.
[17] A. Patnaik, A. Satapathy, S. S. Mahapatra, R. R. Dash, *Mater. Des.* **2009**, *30*, 57.
[18] B. Schemmer, C. Kronenbitter, S. Mecking, *Macromol. Mater. Eng.* **2018**, *303*, 1700416.
[19] Z. Bartczak, M. Grala, E. Richaud, K. Gadzinowska, *Polymer* **2016**, *99*, 552.
[20] R. Kaundal, *Silicon* **2017**, *9*, 223.
[21] C. Wang, M. Zhao, J. Li, J. Yu, S. Sun, S. Ge, X. Guo, F. Xie, B. Jiang, E. Wujcik, Y. Huang, N. Wang, Z. Guo, *Polymer* **2017**, *131*, 263.
[22] S. Biswas, A. Satapathy, *Mater. Des.* **2010**, *31*, 1752.
[23] Z. Wang, H. Zhu, N. Cao, R. Du, Y. Liu, G. Zhao, *Mater. Lett.* **2017**, *186*, 274.
[24] J. W. M. Mens, A. W. J. De Gee, *Tribol. Int.* **1986**, *19*, 59.
[25] S. Soderberg, S. Hogmark, U. Engman, H. Swahn, *Tribol. Int.* **1981**, *14*, 333.
[26] M. Su, X. Zeng, X. Lai, H. Li, *Polym. Test.* **2018**, *65*, 491.
[27] X. Cui, G. Zhu, Y. Pan, Q. Shao, C. Zhao, M. Dong, Y. Zhang, Z. Guo, *Polymer* **2018**, *138*, 203.
[28] A. S. Virk, W. Hall, J. Summerscales, *Compos. Sci. Technol.* **2010**, *70*, 995.
[29] G. Arena, K. Friedrich, D. Acierno, E. Padenko, P. Russo, G. Filippone, J. Wagner, *eXPRESS Polym. Lett.* **2015**, *9*, 166.
[30] Y. Yang, P. Zeng, L. Lei, *J. Appl. Polym. Sci.* **2015**, *132*, 41299.
[31] C. Wang, Z. He, X. Xie, X. Mai, Y. Li, T. Li, M. Zhao, C. Yan, H. Liu, E. Wujcik, Z. Guo, *Macromol. Mater. Eng.* **2018**, *303*, 1700462.
[32] C. Wang, B. Mo, Z. He, Q. Shao, D. Pan, E. Wujick, J. Guo, X. Xie, X. Xie, Z. Guo, *J. Membr. Sci.* **2018**, *556*, 118.
[33] C. Wang, B. Mo, Z. He, C. X. Zhao, L. Zhang, Q. Shao, X. Guo, E. Wujcik, Z. Guo, *Polymer* **2018**, *138*, 363.
[34] Z. Wang, R. Wei, J. Gu, H. Liu, C. Liu, C. Luo, J. Kong, Q. Shao, N. Wang, Z. Guo, X. Liu, *Carbon* **2018**, *139*, 1126.
[35] N. Wu, D. Xu, Z. Wang, F. Wang, J. Liu, W. Liu, Q. Shao, H. Liu, Q. Gao, Z. Guo, *Carbon* **2019**, *145*, 433.
[36] N. Wu, C. Liu, D. Xu, J. Liu, W. Liu, Q. Shao, Z. Guo, *ACS Sustainable Chem. Eng.* **2018**, *6*, 12471.
[37] N. Wu, C. Liu, D. Xu, J. Liu, W. Liu, H. Liu, J. Zhang, W. Xie, Z. Guo, *J. Mater. Chem. C* **2019**, *7*, 1659.
[38] Y. Zhao, L Qi, Y Jin, K. Wang, J. Tian, P. Han, *J. Alloys Compd.* **2015**, *647*, 1104.
[39] C. Hou, Z. Tai, L. Zhao, Y. Zhai, Y. Hou, Y. Fan, F. Dang, J. Wang, H. Liu, *J. Mater. Chem. A* **2018**, *6*, 9723.
[40] K. Xu, C. Liu, K. Kang, Z. Zheng, S. Wang, *Compos. Sci. Technol.* **2018**, *154*, 8.
[41] H. Liu, Q. Li, S. Zhang, R. Yin, X. Liu, Y. He, K. Dai, C. Shan, J. Guo, C. Liu, C. Shen, X. Wang, N. Wang, Z. Wang, R. Wei, Z. Guo, *J. Mater. Chem. C* **2018**, *6*, 12121.
[42] H. Liu, M. Dong, W. Huang, J. Gao, K. Dai, J. Guo, G. Zheng, C. Liu, C. Shen, Z. Guo, *J. Mater. Chem. C* **2017**, *5*, 73.
[43] H. Wei, D. Ding, S. Wei, Z. Guo, *J. Mater. Chem. A* **2013**, *1*, 10805.
[44] J. L. Gadley, R. J. Andrade, J. M. Maia, *Macromol. Mater. Eng.* **2016**, *301*, 953.
[45] W. Cai, X. Mu, Y. Pan, W. Guo, J. Wang, B. Yuan, X. Feng, Q. Tai, Y. Hu, *Polym. Adv. Technol.* **2018**, *29*, 2545.
[46] S. M. Cruz, J. C. Viana, *Macromol. Mater. Eng.* **2015**, *300*, 1153.
[47] J. Guo, H. Song, H. Liu, C. Luo, Y. Ren, T. Ding, M. A. Khan, D. P. Young, X. Liu, X. Zhang, J. Kong, Z. Guo, *J. Mater. Chem. C* **2017**, *5*, 5334.
[48] C. Cheng, R. Fan, Y. Ren, T. Ding, L. Qian, J. Guo, X. Li, L. An, Y. Lei, Y. Yin, Z. Guo, *Nanoscale* **2017**, *9*, 5779.
[49] H. Gu, H. Zhang, C. Ma, X. Xu, Y. Wang, Z. Wang, R. Wei, H. Liu, C. Liu, Q. Shao, X. Mai, Z. Guo, *Carbon* **2019**, *142*, 131.

© 2019 WILEY-VCH Verlag GmbH & Co. KGaA, Weinheim

[50] H. Unal, A. Mimaroglu, *Wear* **2012**, *289*, 132.
[51] K. Sun, P. Xie, Z. Wang, T. Su, Q. Shao, J. Ryu, X. Zhang, J. Guo, A. Shankar, J. Li, R. Fan, D. Cao, Z. Guo, *Polymer* **2017**, *125*, 50.
[52] L. Wang, L. Zhang, M. Tian, *Mater. Des.* **2012**, *39*, 450.
[53] J. Karget-Kocsis, A. Mousa, Z. Major, N. Bekesi, *Wear* **2008**, *264*, 359.
[54] D. Felhos, J. Karget-Kocsis, *Tribol. Int.* **2008**, *41*, 404.
[55] C. Lin, H. Hu, C. Cheng, K. Sun, X. Guo, Q. Shao, J. Li, N. Wang, Z. Guo, *Electrochim. Acta* **2018**, *260*, 65.
[56] K. Sun, P. Xie, Z. Wang, T. Su, Q. Shao, J. Ryu, X. Zhang, J. Guo, A. Shankar, J. Li, R. Fan, D. Cao, Z. Guo, *Polymer* **2017**, *125*, 50.
[57] A. Papadopoulos, G. Gkikas, A.S. Paipetis, N.M. Barkoula, *Composites, Part A* **2016**, *84*, 299.
[58] Y. He, S. Yang, H. Liu, Q. Shao, Q. Chen, C. Lu, Y. Jiang, C. Liu, Z. Guo, *J. Colloid Interface Sci.* **2018**, *517*, 40.
[59] Z. Li, B. Wang, X. Qin, Y. Wang, C. Liu, Q. Shao, N. Wang, J. Zhang, Z. Wang, C. Shen, Z. Guo, *ACS Sustainable Chem. Eng.* **2018**, *6*, 13747.
[60] Z. Wu, H. Cui, L. Chen, D. Jiang, L. Weng, Y. Ma, X. Li, X. Zhang, H. Liu, N. Wang, J. Zhang, Y. Ma, M. Zhang, Y. Huang, Z. Guo, *Compos. Sci. Technol.* **2018**, *164*, 195.
[61] J. Zhang, H. Li, B. Zhou, Y. Li, K. Dai, G. Zheng, C. Liu, Y. Ma, J. Zhang, N. Wang, C. Shen, Z. Guo, *J. Mater. Chem. C* **2018**, *6*, 8360.
[62] K. Zhang, G. Li, L. Feng, N. Wang, J. Guo, K. Sun, K. Yu, J. Zeng, T. Li, Z. Guo, M. Wang, *J. Mater. Chem. C* **2017**, *5*, 9359.
[63] Q. Luo, H. Ma, Q. Hou, Y. Li, J. Ren, X. Dai, Z. Yao, Y. Zhou, L. Xiang, H. Du, H. He, N. Wang, K. Jiang, H. Lin, H. Zhang, Z. Guo, *Adv. Funct. Mater.* **2018**, *28*, 1706777.
[64] C. Hu, Z. Li, J. Gao, K. Dai, G. Zheng, C. Liu, C. Shen, H. Song, Z. Guo, *J. Mater. Chem. C* **2017**, *5*, 2318.
[65] X. Guan, G. Zheng, K. Dai, C. Liu, X. Yan, C. Shen, Z. Guo, *ACS Appl. Mater. Interfaces* **2016**, *8*, 14150.
[66] Y. Zheng, Y. Li, K. Dai, M. Liu, K. Zhou, G. Zheng, C. Liu, C. Shen, *Composites, Part A* **2017**, *101*, 41.
[67] Y. Zheng, Y. Li, Z. Li, Y. Wang, K. Dai, G. Zheng, C. Liu, C. Shen, *Compos. Sci. Technol.* **2017**, *139*, 64.
[68] Q. Zhang, J. Wang, J. Yu, Z. Guo, *Soft Matter.* **2017**, *13*, 3431.
[69] R. W. Seymour, G. M. Estes, S. L. Cooper, *Macromolecules* **1970**, *3*, 579.
[70] H. Xia, M. Song, *Soft Matter* **2005**, *1*, 386.
[71] D. A. Nguyen, Y. R. Lee, A. V. Raghu, H. M. Jeong, C. M. Shin, B. K. Kim, *Polym. Int.* **2009**, *58*, 412.
[72] Z. Gong, J. Gong, X. Yan, S. Gao, B. Wang, *J. Phys. Chem. C* **2011**, *115*, 18468.
[73] V. A. Bershtein, L. M. Egorova, P. N. Yakushev, P. Pissis, P. Sysel, L. Brozova, *J. Polym. Sci., Part B: Polym. Phys.* **2002**, *40*, 1056.
[74] C. Leu, Y. Chang, K. Wei, *Chem. Mater.* **2003**, *15*, 3721.
[75] S. Jin, D. Choi, D. Lee, *Colloids Surf. A* **2008**, *313–314*, 242.
[76] A. Montazeri, K. Pourshamsian, M. Riazian, *Mater. Des. (1980–2015)* **2012**, *36*, 408.
[77] J. Zhu, S. Wei, Y. Li, L. Sun, N. Haldolaarachchige, D. P. Young, C. Southworth, A. Khasanov, Z. Luo, Z. Guo, *Macromolecules* **2011**, *44*, 4382.
[78] Q. He, T. Yuan, J. Zhu, Z. Luo, N. Haldolaarachchige, L. Sun, A. Khasanov, Y. Li, D. P.Young, S. Wei, Z. Guo, *Polymer* **2012**, *53*, 3642.
[79] P. Russo, D. Acierno, G. Marletta, G. L. Destri, *Eur. Polym. J.* **2013**, *49*, 3155.
[80] E. Badamshina, Y. Estrin, M. Gafurova, *J. Mater. Chem. A* **2013**, *1*, 6509.
[81] U. Khan, P. May, A. O'Neill, J. J. Vilatela, A. H. Windle, J. N. Coleman, *Small* **2011**, *7*, 1579.
[82] X. Cao, X. Wei, G. Li, C. Hu, D. Kun, J. Guo, G. Zheng, C. Liu, C. Shen, Z. Guo, *Polymer* **2017**, *112*, 1.
[83] V. Kumar, D. Lee, *Polym. Adv. Technol.* **2017**, *28*, 1842.
[84] Y. Cao, J. Feng, P. Wu, *Carbon* **2010**, *48*, 3834.
[85] X. Wang, Y. Hu, L. Song, H. Yang, W. Xing, H. Lu, *J. Mater. Chem.* **2011**, *21*, 4222.
[86] N. M. Barkoula, J. Karget-Kocsis, *J. Mater. Sci.* **2002**, *37*, 3807.
[87] H. M. Clark, K. K. Wong, *Wear* **1995**, *186–187*, 454.
[88] J. G. A. Bitter, *Wear* **1963**, *6*, 5.
[89] I. M. Hutchings, *Powder Technol.* **1993**, *76*, 3.
[90] R. G. Wellman, J. R. Nicholls, *J. Phys. D: Appl. Phys.* **2007**, *40*, R293.
[91] K. H. Zum Gahr, *Tribol. Int.* **1998**, *31*, 587.
[92] J. Li, I. M. Hutchings, *Wear* **1990**, *135*, 293.
[93] R. K. Kumar, S. Seetharamu, M. Kamaraj, *Wear* **2014**, *320*, 16.

© 2019 WILEY-VCH Verlag GmbH & Co. KGaA, Weinheim